High Ion Conductive and Selective Membrane Achieved through Dual Ion Conducting Mechanisms

Tongtai Ji, Chunyan Zhang, Xianghui Xiao, Ying Wang, Daxian Cao, Arturas Adomkevicius, Yuyue Zhao, Xiao Sun, Kun Fu, and Hongli Zhu*

Conventional ion-selective membranes, that is ion-exchange and porous membranes, are unable to perform high conductivity and selectivity simultaneously due to the contradictions between their ion selecting and conducting mechanisms. In this work, a bifunctional ion-selective layer is developed via the combination of nanoporous boron nitride (PBN) and ion exchange groups from Nafion to achieve high ion conductivity through dual ion conducting mechanisms as well as high ion selectivity. A template-free method is adopted to synthesize flake-like PBN, which is further enmeshed with Nafion resin to form the bifunctional layer coated onto a porous polyetherimide membrane. The double-layer membrane exhibits excellent ion selectivity (1.49×10^8 mS cm^{-3} min), which is 22 times greater than that of the pristine porous polyetherimide membrane, with outstanding ion conductivity (64 mS cm^{-1}). In a vanadium flow battery, the double-layer membrane achieves a high Coulombic efficiency of 97% and outstanding energy efficiency of 91% at 40 mA cm^{-2} with a stable cycling performance for over 700 cycles at 100 mA cm^{-2}. PBN with ion exchange groups may therefore offer a potential solution to the limitation between ion selectivity and conductivity in ion-selective membranes.

1. Introduction

Flow batteries have attracted considerable attention as a large-scale energy storage technology because of their unique feature of uncoupling power and energy, which allows the expansion of energy storage by increasing the volume or concentration of the electrolyte.[1] Compared with other electrochemical technologies,

T. Ji, Y. Wang, D. Cao, A. Adomkevicius, Y. Zhao, X. Sun, H. Zhu
Department of Mechanical and Industrial Engineering
Northeastern University
Boston, MA 02115, USA
E-mail: h.zhu@neu.edu
C. Zhang, K. Fu
Department of Mechanical Engineering
University of Delaware
Newark, DE 19716, USA
X. Xiao
National Synchrotron Light Source II
Brookhaven National Laboratory
Upton, NY 11973, USA

such as lead-acid, lithium-ion, and sodium-based batteries, flow batteries have the advantages of long life, high safety, and low cost.[2] An ion-selective membrane is an essential part of flow batteries. On the one side, the membrane allows specific ions to pass through, maintaining a neutral charge in the cell.[3] On the other side, it prevents the crossover of active species to maintain the capacity. The properties of the ion-selective membrane have a significant impact on the flow battery's performance. The ideal ion-selective membranes should have high ion conductivity and selectivity, high chemical stability, good mechanical strength, and low cost.[4]

Based on the ion-selective and conductive mechanisms, conventional ion-selective membranes can be classified into ion-exchange and porous membranes.[4,5] The ion-exchange membranes can be categorised as cation (with anion groups) and anion (with cation groups) exchange membranes according to the conduciton of different ions based on Donnan exclusion mechanism.[5b] The Nafion membrane is one of the most common cation exchange membranes used in flow batteries. Nafion consists of polytetrafluoroethylene main chains and side chains containing superacidic sulfonic acid groups.[6] Hydrophilic sulfonic acid groups constitute ion-transmission channels that provide excellent cation conductivity. However, Nafion membranes have a heavy crossover issue due to the large amount of cation active species involved in the flow batteries, as well as the high cost of the Nafion membranes hindering their commercial application on large scale.[3,7] Sulfonated poly (ether ketone) (SPEEK) is an attractive material of ion exchange membrane with relatively low cost and high stability.[8] In comparison with Nafion, SPEEK has a higher ion selectivity because of the less acidic sulfonic acid groups and hydrophobic PEEK backbone; however, the ion conductive channels are relatively tortuous.[9] Normally, a high sulfonation degree of SPEEK is required in order to achieve sufficient ion conductivity. However, this can lead to swelling, decreases stability, as well as reduced ion selectivity.[6,9] Over the past decade, porous membranes have been used as ion-selective membranes in flow batteries because of their low cost, high stability, and high ion conductivity.[10] Porous membrane transport ions through pores or channels, and the ion selectivity is governed by the pore size exclusion mechanism.

**ADVANCED
SCIENCE NEWS**
www.advancedsciencenews.com

NANO · MICRO
small
www.small-journal.com

Porous membranes perpared through non-solvent induced phase separation (NIPS) method exhibit asymmetric finger-like pores in the vertical direction with thin surface layers on the top and bottom of the membranes attracting great attentions. Vertical finger-like pores provide excellent and unhindered ion transfer, and the ion selectivity is mainly attributable to the pore morphology in the surface layer.[10] Ideally, a dense and thick surface layer should be formed to achieve high ion selectivity, but in doing so it also reduces the size and density of the vertical pores, which is detrimental to the ion conductivity of the membrane.[10c] In summary, traditional ion-exchange and porous membranes require a trade-off between ion selectivity and conductivity.

Boron nitride (BN), also known as white graphite, exhibits superior chemical and thermal stability, high thermal conductivity, and excellent electrical insulating properties.[11] Further to the advantages of BN, nanoporous BN (PBN) has a ultra-high and adjustable nanoporosity, thus being useful for multiple applications, such as absorption, separation, and chemical conversion.[12] With its high nanoporosity and stability, PBN has the potential to be an attractive material for ion selective. PBN can be obtained through three bottom-up methods: chemical blowing,[13] template-based,[14] and template-free[15] techniques. The template-free approach has several advantages over chemical blowing or template-based approaches, including a simple synthesis procedure, low costs, and relatively low toxicity.[16] For the template-free method, PBN is synthesized by reacting boron-containing and excess nitrogen-containing precursors at high temperatures. Nanopores are formed through the decomposition and release of excess nitrogen precursors during the synthesis process.[15f] The porosity and morphology of PBN can be tailored by varying different types or proportions of precursors and changing reaction conditions.[15b,e]

Inspired by the features of different ion-selective membranes and PBN, we have developed a double-layer ion-selective membrane with a unique PBN bifunctional ion-selective layer on a low-cost and highly ion-conductive porous polyetherimide (PEI) layer. As a first step, PBN was synthesized using a template-free method with a stacked flake-like shape and nanoporous structure. In the dispersion process of PBN flakes, the hydrophilicity and crystallinity of the PBN were increased simultaneously by sonication in isopropanol, as showed by X-ray diffraction (XRD), Fourier transform infrared (FTIR) spectroscopy, thermogravimetric analysis (TGA), and contact angle measurements. The nanoporosity of PBN was characterized using the N2 adsorption-desorption technique and calculated using non-local density functional theory (NLDFT). PBN was further mixed with Nafion resin and spray-coated onto the porous PEI membrane prepared by the NIPS method to form a PBN–PEI double-layer membrane. The morphology and properties of the PBN–PEI membrane were investigated in order to identify its ion-selective and ion-conductive mechanisms. Furthermore, the electrochemical performance of the membrane was evaluated in a vanadium redox flow battery (VRFB). The unique PBN bifunctional ion-selective layer with the nanoporous structure and ion-exchange groups overcomes the limitation between ion conductivity and selectivity in conventional ion-selective membranes. More importantly, the overlap of the novel bifunctional PBN ion selective layer with the low-cost high ion-conducting PEI layer demonstrated superior performance due to its ability to integrate the advantages of both layers.

2. Results and Discussions

Figure 1a illustrates the functionality of the PBN–PEI double-layer membrane in a VRFB, which allows proton transfer and suppresses the crossover of vanadium ions. The PEI layer was prepared using the NIPS method with an extensive network of longitudinal unimpeded finger-like pores, resulting in superior ion conductivity (Figure 1b). In addition, the PEI layer provides decent mechanical support for the ultra-thin PBN layer ($\approx$ 5 μm). The PBN layer is composed of PBN flakes decorated with Nafion resin (Figure 1c). Accordingly, the nano-sized and tortuous pores of the PBN flakes can effectively block the crossover of vanadium ions and provide excellent ion selectivity based on the pore size exclusion mechanism. Furthermore, the super-acidic sulfonic acid groups of Nafion decorated on the nanoporous structure of PBN provide high-speed proton transfer channels that increase proton conductivity through both Grotthuss and vehicle mechanisms (Figure 1d).[17] Furthermore, the double-layer design of the PBN-PEI membranes with a low-cost PEI supporting layer and a ultra-thin PBN ion-selective layer, results in a significant reduction of cost when compared to the Nafion 115 membrane (Table S1, Supporting Information), which can be beneficial to the commercialization and advancement of PBN-PEI membranes. Overall, the PBN–PEI membrane can achieve high ion selectivity, ion conductivity, stability, and low cost.
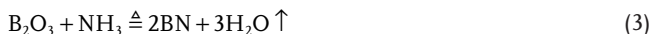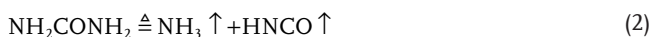
For the preparation of the low-cost and highly ion-conductive PEI membrane using the NIPS method, polyvinylpyrrolidone (PVP) was added as a hydrophilic polymer additive to further improve ion conductivity.[10d] The porous PEI membrane presented a smooth and flat surface (Figure S1, Supporting Information) with a contact angle of 71° (Figure S2, Supporting Information). The scanning electron microscopy (SEM) images (**Figure 2**a,b) revealed a dense top surface and a porous crosssection with asymmetric finger-like pores in the PEI membrane. The PEI membrane's 3D structure was reconstructed using micro X-ray computed tomography (XCT), as illustrated in Figure 2c (top surface was removed to disclose the internal structure). The unobstructed channels of the well-aligned asymmetric finger-like pores provided excellent ion conductivity. Furthermore, the high-magnification SEM image (Figure S3, Supporting Information) revealed the presence of a substantial number of secondary pores on the pore walls. These secondary pores further enhanced the ion conductivity of the porous PEI membrane. The PEI membrane was exposed for one week to the high acidic vanadium electrolyte (1 M VOSO4 and 3 M H2SO4) and characterized using XRD and FTIR (Figure S4, Supporting Information) to determine its chemical stability. It was found that no apparent differences were observed, demonstrating that the PEI membrane could be used as the support layer in a strongly acidic environment.

PBN was synthesized by the template-free method with a precursor of boric acid and excess urea through the reactions as shown in Equations (1–3)[12c,15c,f]
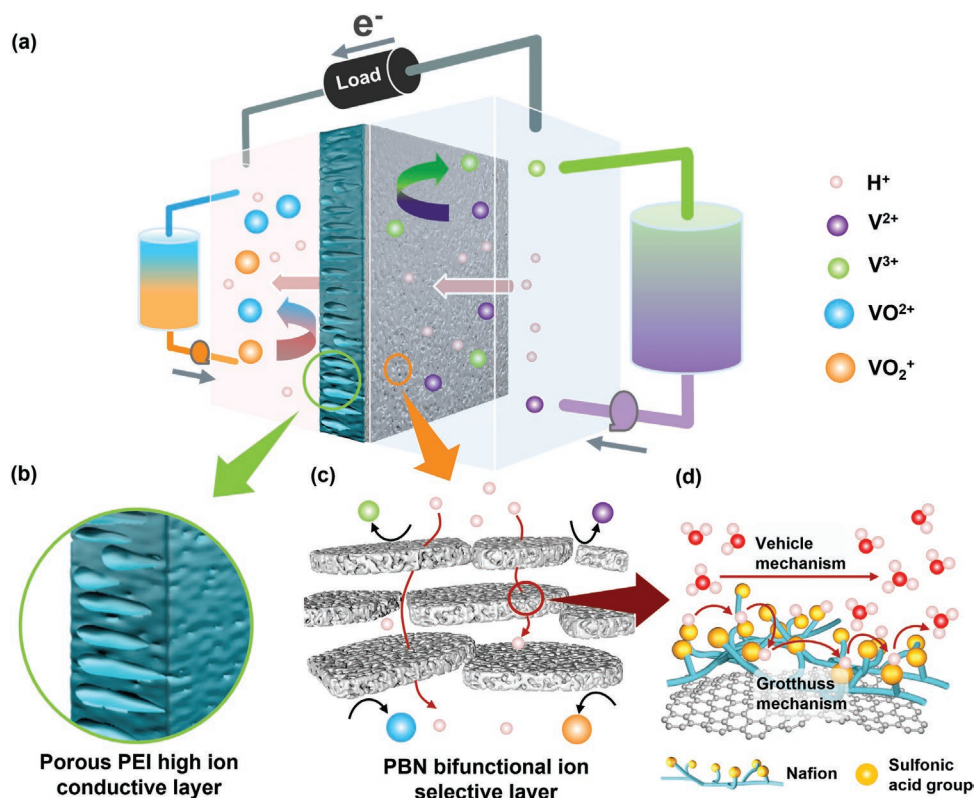
Figure 1. a) Schematic of the two-layer PBN–PEI membrane in VRFB. The blue and white layers represent the PEI highly ion-conductive and PBN bifunctional ion-selective layers, respectively. b) Schematic of the PEI highly ion-conductive supporting layer. c) Schematic of the PBN ion-selective layer. d) Schematic of the proton conduction mechanisms in the PBN layer.
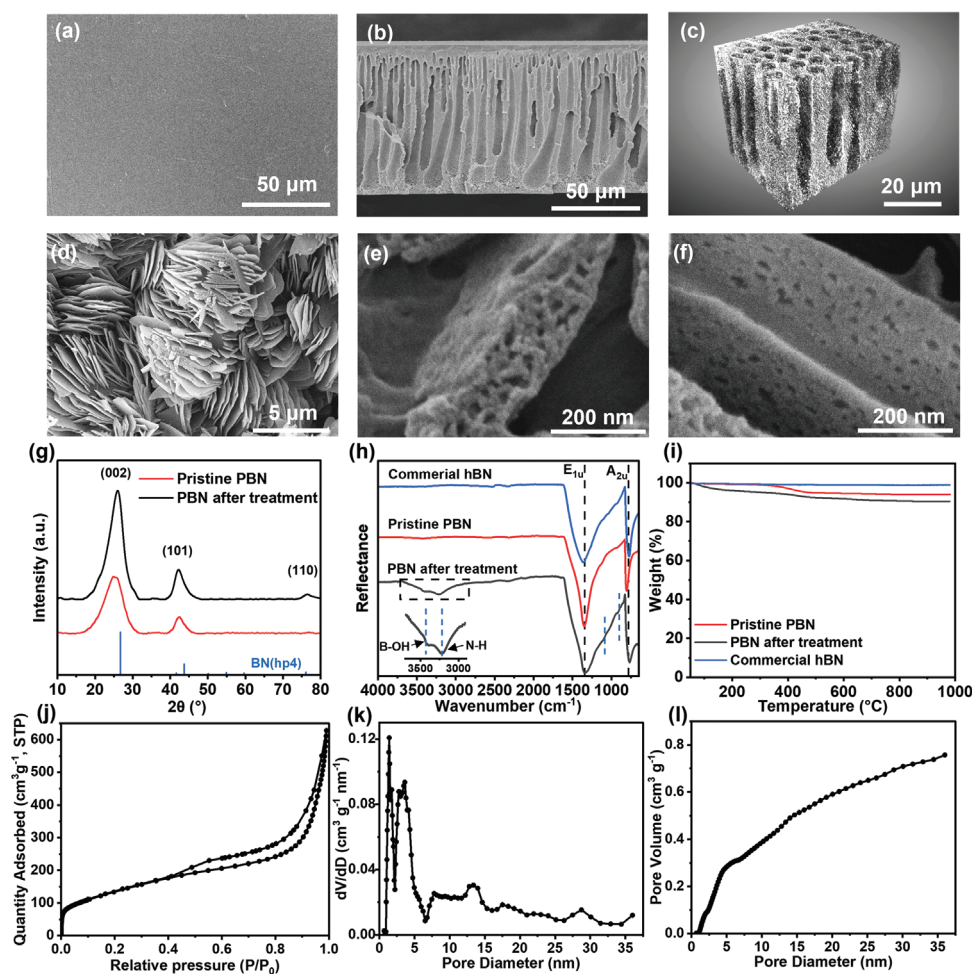
$$2H_3BO_3 \triangleq B_2O_3 + 3H_2O \uparrow \qquad (1)$$

$$NH_2CONH_2 \triangleq NH_3 \uparrow + HNCO \uparrow \qquad (2)$$

$$B_2O_3 + NH_3 \triangleq 2BN + 3H_2O \uparrow \qquad (3)$$

The nanoporosity is attributed to the generation and release of gaseous products during the reaction.[15f] As shown in the SEM image (Figure 2d), the PBN consists of multiple stacked PBN flakes. High-magnification SEM images of the PBN flakes (Figure 2e,f) reveal continuous nanoporous structures throughout their cross-section and surface.

PBN flakes were obtained by grinding and sonicating pristine PBN in isopropanol, followed by centrifugation and filtration. In addition, PBN was also modified during the sonication process. PBN was compared before and after treatment, using SEM, XRD, FTIR, and TGA results to investigate the effects and mechanisms of treatment. Figure 2g shows the XRD spectra of PBN before and after treatment with three characteristic peaks corresponding to the (002), (101), and (110) planes of hexagonal BN (hBN) (PDF#45-0894). The broad characteristic peaks show that PBN contained amorphous BN. As a result of the treatment, the peak (002) became sharper and the full-width half maximum of the peak decreased from 5.953 to 5.066, indicating the removal of some amorphous BN. The crystallinity of PBN increased from 12.26% to 18.62% as calculated based on the (002) peak by MDI Jade XRD software.

According to the FTIR spectra shown in (Figure 2h), BN typically has two characteristic peaks: the E_{1u} peak at 1403 cm^{-1} produced by in-plane oscillation within the BN plane (B−N stretching) and the A_{2u} peak at 808 cm^{-1} caused by the c-axis vibration (B−N−B bending).[18] After treatment, the intensity ratio of A_{2u} and E_{1u} of PBN increased and was comparable to that of hBN. It appears that PBN exhibits more characteristics of hBN as a result of the decomposition of some amorphous BN during the treatment process, as confirmed by the XRD analysis. Following the treatment, two broad peaks were observed at 3000–3600 cm^{-1}, which corresponded to the B−OH and N−H stretching, respectively.[19] The peaks at 1100 and 992 cm^{-1} related to the B−O linkage were strengthed.[11] The appearance and strengthening of these peaks indicated the successful introduction of the hydroxyl and amino groups into PBN. The process of the functionalization of PBN is similar to the edge functionalization of hBN, where the solvent molecules attack the B−N bonds near the defects or edges, and the functional groups are introduced upon exposure of the new edges.[20] As amorphous BN contains a significantly higher ratio of defects than hBN, functionalization is more efficient.[13b]

TGA was performed to further verify the functionalization of PBN. Compared to commercial hBN, pristine PBN showed an approximate weight loss of 4.8% as a result of the thermal degradation of some amorphous BN after 300 °C. Nevertheless, the treated PBN lost 4.9% of its weight loss before 300 °C, indicating the functional groups had successfully been introduced

**ADVANCED
SCIENCE NEWS**

www.advancedsciencenews.com

**NANO · MICRO
small**

www.small-journal.com

Figure 2. SEM images of a) the top surface and b) the cross-section of the PEI membrane. c) XCT 3D reconstruction of the PEI membrane (the top surface was removed). d–f) SEM images of pristine PBN. g) XRD spectra of pristine PBN, PBN after treatment, and BN (hp4) (PDF#45-0894). h) FTIR spectra of PBN before and after treatment. i) TGA of pristine PBN, PBN after treatment, and commercial hBN. j) Nitrogen adsorption-desorption isotherm, k) pore size distribution by the NLDFT method, and l) cumulative pore volume of PBN after treatment.

(Figure 2i).[11] The PBN after treatment exhibited excellent thermal stability and maintained 90% of its initial weight at 1000 °C. The hydrophilic properties of pristine and treated PBN were evaluated by compressing them into pallets and measuring their contact angles (Figure S5a, Supporting Information).[21] The contact angle of PBN after treatment was significantly smaller than that of pristine PBN, as shown in Figure S5b,c, Supporting Information, which suggests the improved hydrophilicity of PBN with the introduction of hydroxyl and amino groups after treatment.

The pore size distribution (PSD) and pore volume of the PBN were evaluated by the N_2 adsorption–desorption method. Based on the standards of the International Union of Pure and Applied Chemistry (IUPAC), both pristine and treated PBN exhibited type I and IV isotherms with type H3 and H4 hysteresis loops (Figure S6a, Supporting Information, and Figure 2j),[22] which indicate the presence of micropores and mesopores with spherical and split morphologies in PBN. The NLDFT method was used to calculate the PSDs of the PBNs.[15d] The pristine PBN exhibited a bimodal PSD with several broad peaks in the 10–35 nm range (Figure S6b, Supporting

Information), which are consistent with the pores observed in the SEM image (Figure 2e,f). After treatment, PBN still exhibited a bimodal PSD, in which the right peak became broader but lower and left-shifted to 3.3 nm (Figure 2k). The change in the PSDs and analysis of the treatment process indicate that a certain volume of pores is provided by the amorphous component of PBN. During the treatment process, some of the loose amorphous part was decomposed, and the firmer amorphous part with smaller pore sizes was left. As shown in Figure 2l, the pore volume of the PBN after treatment, the mesopore volume was maintained at 0.76 cm³ g⁻¹, and ≈ 37% of the pores were smaller than 5 nm (0.28 cm³ g⁻¹), further supporting that PBN has an excellent ion selectivity based on the pore size exclusion mechanism.

PBN was further dispersed in Nafion solution and spray coated onto the PEI membrane, where Nafion was used as binder and ion exchange group supplier to form the bifunctional ion-selective layer (See Figures S7 and S8, Supporting Information). The ratio of PBN to Nafion directly affects the morphology and properties of the PBN layer (**Figure 3**a). To explore the optimal ratio, three PBN layers with different
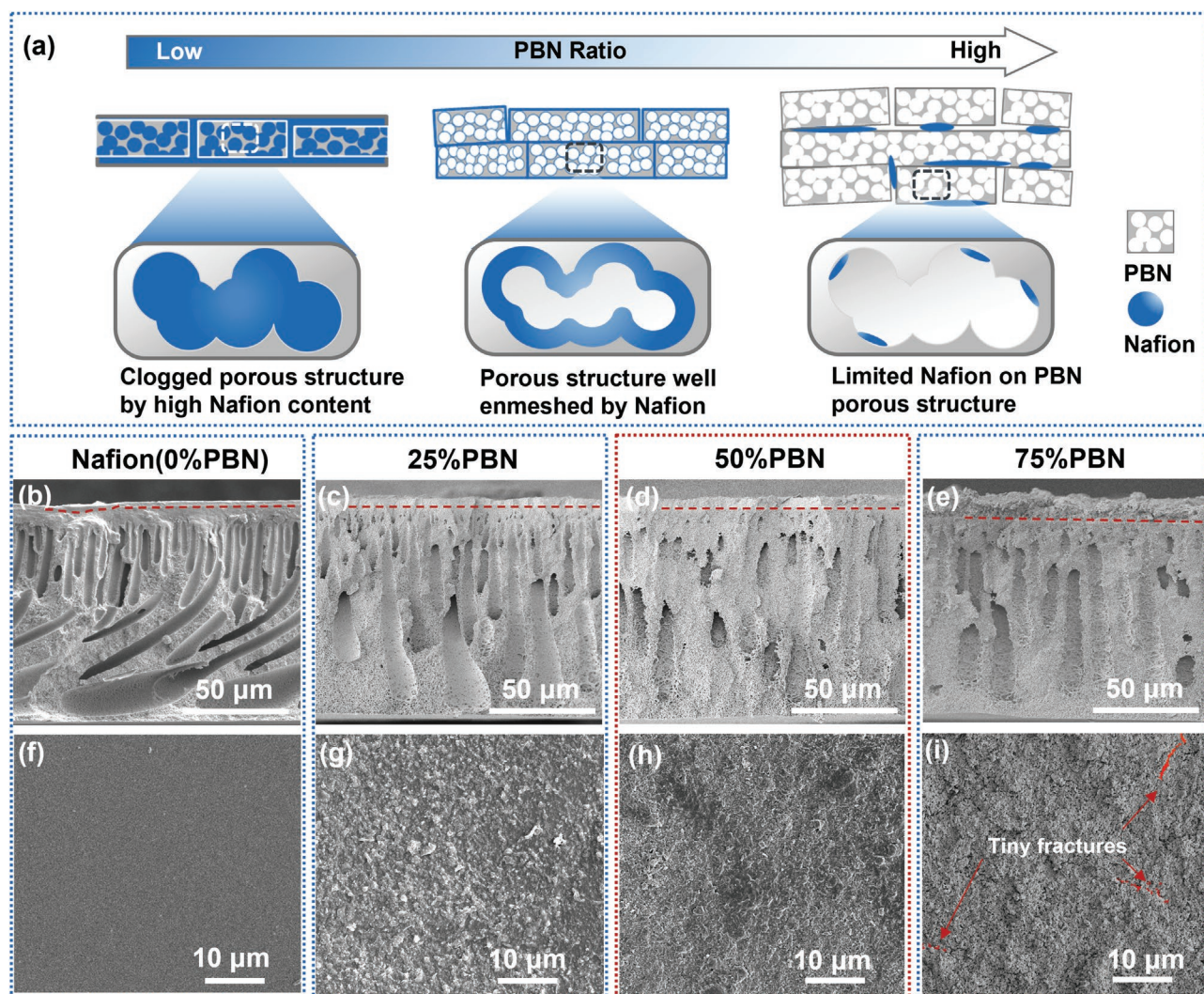
Figure 3. a) Schematic of the PBN layer with different PBN ratio. SEM images of the cross-sections of the b) Nafion-PEI (0%PBN-PEI), c) 25%PBN–PEI, d) 50%PBN–PEI, and e) 75%PBN–PEI membranes. SEM images of the top surfaces of the f) 0%PBN-PEI(Nafion-PEI), g) 25%PBN–PEI, h) 50%PBN–PEI, and i) 75%PBN–PEI membranes.

PBN–Nafion weight ratios (25%, 50%, and 75%) were prepared (as shown in Table S2, Supporting Information). As a means of evaluating the contribution of Nafion resin, a Nafion-PEI (0%PBN-PEI) membrane was also prepared. SEM was used to evaluate the morphologies of the pure Nafion (0%PBN) layer and PBN layers with different PBN ratios. PBN and Nafion were uniformly deposited on the top surface of the PEI membranes, as shown in Figure 3b–e. The thicknesses of the Nafion, 25%PBN, 50%PBN, and 75%PBN layers were ≈ 2, 3, 5, and 7 µm, respectively (Figure S9a–d, Supporting Information) because of the difference in the densities of the PBN and Nafion resin. An interface layer, in addition to the 2 µm coating layer, was observed on the cross-section of the Nafion-PEI membrane due to the infiltration of the Nafion resin into the PEI membrane (Figure S9a, Supporting Information). This phenomenon was not found in PBN-PEI membrane, which indicated Nafion resin was well enmeshed with PBN. The 25%PBN and 50%PBN layers appeared dense cross-sectional morphologies with no distinct gaps (Figure S9f,g, Supporting Information). The cross-section of the 75%PBN layer (Figure S9h, Supporting Information) was less condensed with more pores due to the lower amount of Nafion resin. Figure 3f–i is the SEM images of the top surfaces of the coating layers. The Nafion (0%PBN) layer shows a flat and nonporous surface (Figure 3f). However, there were tiny fissures observed on the top surface of the 75%PBN layer (Figure 3i) as a result of the limited Nafion resin (25%), which was unable to tightly bind the PBN flakes together. Figure S9g–l, Supporting Information, shows high-magnification images of the 25%, 50%, and 75%PBN layers, which exhibit different morphologies. As can be seen in Figure S9g, Supporting Information, the top surface of the 25%PBN layer was fully covered with Nafion resin, with no visible gaps or pores. In the case of the 50%PBN layer (Figure S9k, Supporting Information), the PBN flakes were well enclosed by the Nafion resin with very few pores and openings visible. In the 75%PBN layer (Figure S9i, Supporting Information), the

ADVANCED
SCIENCE NEWS
www.advancedsciencenews.com

NANO · MICRO
small
www.small-journal.com

top surface was rougher, and it is difficult to detect the presence of Nafion resin.

PBN–PEI membranes were characterized to determine their composition, hydrophilicity, water uptake, swelling ratio, mechanical properties, ion conductivity, and selectivity. Based on the FTIR spectrum (Figure S10, Supporting Information), all PBN layers exhibit peaks corresponding to the composition of PBN and Nafion, demonstrating the successful coating of the PBN layers. Contact angle measurements were used to characterize the hydrophilicity of the PBN layers. As a result of the hydrophobicity of PBN and the roughness of the surface, the contact angles of the PBN layers increase with the rise in the PBN ratio (from 25% to 75%), as shown in **Figure 4**a. The water uptake and swelling ratios are shown in Figure 4b. The water uptake of the PBN–PEI membranes is primarily attributed to the PEI layer because of the high porosity of the PEI

layer and the extreme thinness of the PBN layer. This results in similar water uptake values of the membranes. The nonporous structure of the Nafion coating layer and the filled interface layer contribute to the slightly lower water uptake of the Nafion-PEI membrane. In terms of the swelling ratio, all PBN–PEI membranes exhibited lower swelling ratios than pristine PEI and Nafion 115 membranes. The rigid PBN flakes suppressed the movement of the polymer chains in the PBN layer and reduced the swelling. Nevertheless, it should be noted that the low swelling ratio of the PBN-PEI double-layer membrane is also related to the fabrication process, where the PBN layer was coated onto the wet PEI membrane in a swelling state, and the membrane was further dried after coating. Therefore, both swelling and shrinkage of the PEI layer were limited by the PBN layer resulting in a low swelling ratio of PBN-PEI membrane. The swelling ratio of the PBN–PEI
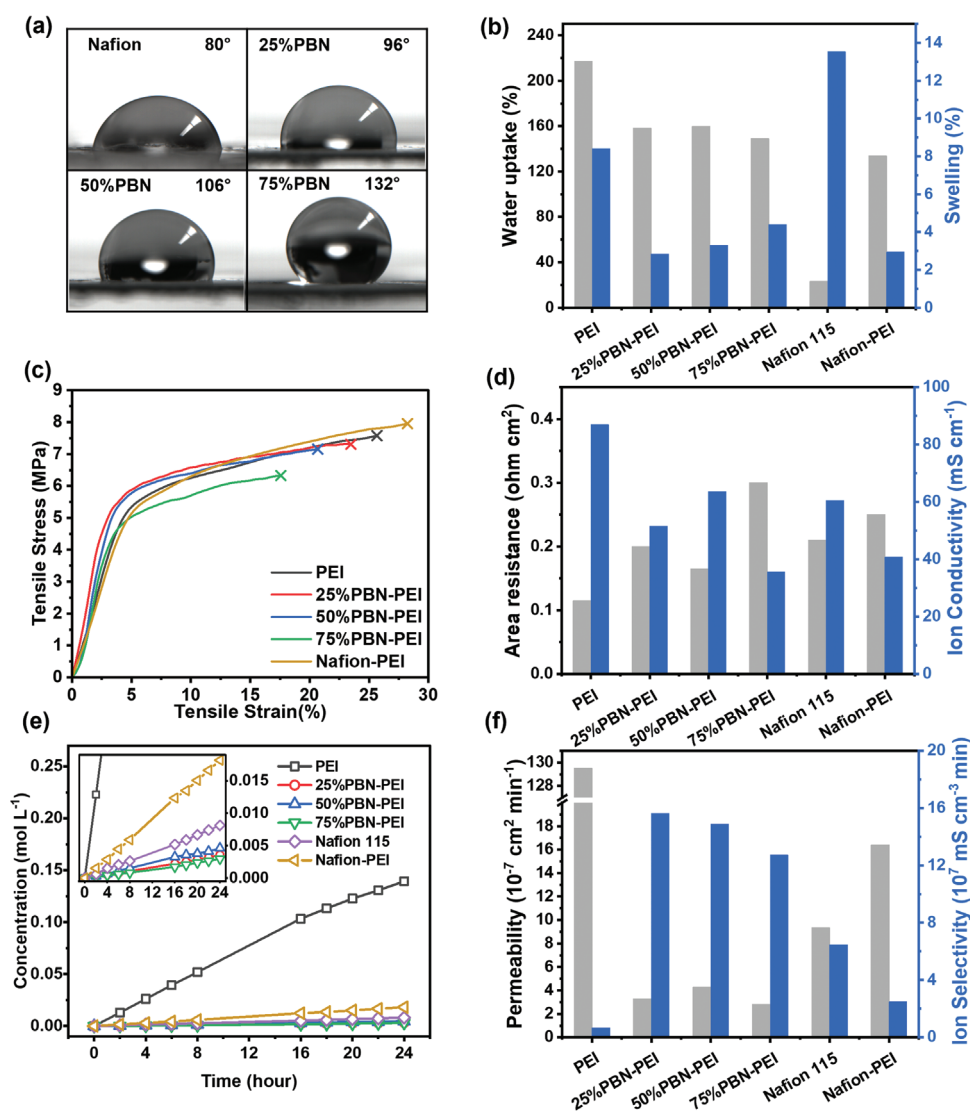
Figure 4. a) Contact angles of Nafion and various PBN layers. b) Water uptake and swelling ratio of the pristine PEI, various PBN–PEI, Nafion-PEI, and Nafion 115 membranes. c) Stress–strain curves of the pristine PEI, various PBN-PEI membranes, and Nafion-PEI membrane. d) Area resistance and ion conductivity, e) time-dependent vanadium ion concentration, and f) vanadium (IV) permeabilities and ion selectivity of the pristine PEI, various PBN–PEI, Nafion-PEI, and Nafion 115 membranes.

**ADVANCED
SCIENCE NEWS**

www.advancedsciencenews.com

NANO · MICRO

small

www.small-journal.com

membrane slightly increased with an increase in the PBN ratio. This is because less Nafion could not provide enough mechanical strength in the PBN layer to fully resist the swelling of the PEI membrane. Correspondingly, small fractures can also be seen in the SEM image of the top surface of the 75%PBN–PEI layer (Figure 3c). Nafion-PEI membrane also presented a lower swelling ratio than the pristine PEI and Nafion 115 membranes due to the filled interface layer restricting the shrinkage of the PEI layer after dehydration.

The mechanical properties of the membrane strongly influenced long-term stability of the flow battery. Good mechanical properties such as high tensile strength and ductility help to prevent membrane deterioration resulting from structural damage during use. The stress–strain curves for the pristine PEI, PBN–PEI, and Nafion 115 membranes are shown in Figure 4c and Figure S11, Supporting Information. Despite the high porous nature of the pristine PEI membrane, the membrane still retains a ductile behavior with good tensile strength (7.58 MPa at 25.7%). The 25%PBN–PEI and 50%PBN–PEI membranes showed higher Young's moduli (176 and 158 MPa, respectively), compared to the pristine PEI and Nafion-PEI membranes (130 and 119 MPa). However, a slightly lower tensile strength and elongation at break (7.30 MPa at 23.47% and 7.16 MPa at 20.68%) was noted. The 25%PBN and 50%PBN layers exhibit increased hardness and lower elasticity compared with the pristine PEI and Nafion-PEI membranes. Despite a fragile morphology observed in the SEM images for the 75%PBN–PEI membrane (Figure 3h,p), the membrane still exhibited a satisfactory tensile strength (6.32 MPa), indicating that the PEI layer provided sufficient structural support. Consequently, PBN–PEI membranes are advantageous for VRFB stability due to their favorable mechanical properties.

Ion conductivity and selectivity are the most significant characteristics of ion-selective membranes, which determine the area resistance and ion permeability of the membrane, thereby affecting the electrochemical performance of the flow battery. The area resistance of all membranes were measured using electrochemical impedance spectroscopy (See Figure S12, Supporting Information) and the ion conductivity were calculated, as shown in Figure 4d. The pristine PEI membrane exhibited the highest ion conductivity (87 mS cm^{-1}) and lowest area resistance (0.115 Ω cm^2) of all membranes owing to the unimpeded ion transfer channels provided by a large number of vertical finger-like pores. It was found that the area resistance of the PBN-PEI membranes increased after the PBN layers were coated. Nevertheless, ion conductivity and area resistance did not correlate linearly with the PBN ratio. The 50%PBN–PEI membrane had the highest ion conductivity (64 mS cm^{-1}) and lowest area resistance (0.165 Ω cm^2) among all other PBN-PEI membranes. The 25%PBN–PEI, 75%PBN–PEI, and Nafion-PEI membranes exhibited lower ion conductivities of 52, 36, and 41 mS cm^{-1}, and higher area resistances of 0.200, 0.295, and 0.250 Ω cm^2, respectively. The ionic conductivity of the PBN layers can be evaluated by subtracting the areal resistance of the pristine PEI membrane from that of the PBN-PEI double-layer membrane, assuming the PBN and PEI layers are connected in series. Further calculations of the ion conductivities of PBN layers are shown in Figure S13, Supporting Information.

Compared to 25%PBN and 75%PBN layers, the 50%PBN layer exhibits a much higher ion conductivity.

Using the morphology and properties of the PBN-PEI membranes, a relationship between the PBN ratio and ion conductivity was examined. Nafion resin with super acidic sulfonic acid groups was successfully introduced into the PBN structure in all the PBN layers. It was found that when the PBN ratio was too low, that is, with a high Nafion content, the Nafion resin clogged the porous structure. Consequently, the rigid structure of PBN could not provide additional space for the sulfonic acid groups to uptake water, resulting in limited proton conductivity.[23] With a medium PBN ratio, the PBN structure was still well enmeshed by the Nafion resin with sufficient space for sulfonic acid groups to uptake water. This resulted in excellent proton conductivity based on both the vehicle and Grotthuss mechanisms.[17] With an excessively high PBN ratio, the limited sulfonic acid groups and hydrophobicity of PBN did not provide high proton conductivity. Due to the filled interface layer in the Nafion-PEI membrane, proton transfer channels were blocked, resulting in a decrease in ion conductivity. Hence, the PBN layer with an appropriate PBN ratio was able to efficiently utilize the ion-exchange groups from the Nafion resin and maintained its porous structure to provide excellent ion conductivity.

The vanadium (IV) permeabilities of all the membranes were calculated based on the results of the vanadium penetration test (Figure 4e) in an H-cell (Figure S14, Supporting Information). The permeabilities of all the membranes are shown in Figure 4f. The PEI membrane experienced a heavy crossover issue with the highest permeability (129 × 10^{-7} cm^2 min^{-1}) because the vertical unblocked pores could not impede the crossover of the vanadium ions. The PBN–PEI membranes exhibit significantly lower permeabilities (3.29 × 10^{-7}, 4.27 × 10^{-7}, and 2.80 × 10^{-7} cm^2 min^{-1} for the 25%PBN–PEI, 50%PBN–PEI, and 75%PBN–PEI membrane) than that of the pristine PEI and Nafion 115 (9.34 × 10^{-7} cm^2 min^{-1}) membranes, which indicates that the PBN layer effectively prevented the crossover of the vanadium ions owing to its nanoporous structure and hydrophobicity. In contrast, the pure Nafion coating on the Nafion-PEI membrane is only able to limit the crossover of the vanadium ions to a small extent and still exhibits high permeability (16.41 × 10^{-7} cm^2 min^{-1}). Furthermore, based on the morphology, thickness, and hydrophilicity discussed above, the 25%PBN layer was more clogged, whereas the 75%PBN layer was more hydrophobic and thicker. This resulted in a slightly lower permeability for the 25%PBN–PEI and 75%PBN–PEI membranes than the 50%PBN–PEI membrane.

The ion selectivity of the membranes was calculated, as shown in Figure 4f. The ion selectivity of the 25%PBN–PEI (1.56 × 10^8 mS cm^{-3} min), 50%PBN–PEI (1.49 × 10^8 mS cm^{-3} min), and 75%PBN–PEI (1.27 × 10^8 mS cm^{-3} min) membranes are ≈ 20 times higher than that of the pristine PEI membrane (6.71 × 10^6 mS cm^{-3} min) and also much higher than that of Nafion 115 (6.48 × 10^7 mS cm^{-3} min) and Nafion-PEI (2.49 × 10^7 mS cm^{-3} min) membranes, which further demonstrates the high contribution of the PBN layer to the ion selectivity of the double-layer membrane. Moreover, the ion selectivity of the PBN–PEI membrane increased with a decrease in the PBN ratio. This phenomenon indicates that the Nafion resin modified the size of the gaps between the PBN flakes

and pores in the PBN structure, thereby further affecting the ion selectivity of the PBN–PEI membrane. In comparison with Nafion 115, the 50%PBN–PEI membrane exhibited lower area resistance, enhanced ion conductivity, lower vanadium permeability, and higher ion selectivity. This resulted in its superior performance when used in VRFBs.

Since the excellent properties of the 50%PBN-PEI membrane, the comprehensive electrochemical performance of the membrane was further evaluated in the VRFB and compared with those of the PEI, Nafion-PEI, and Nafion 115 membranes. The discharge capacities are shown in **Figure 5**a. As expected, the battery assembled with the 50%PBN–PEI membrane exhibited the best rate performance and highest discharge capacities at all current densities (25.4, 24.4, 23.2, 21.8, 20.3, 16.5, and 11.7 Ah L^{-1} at 40, 60, 80, 100, 120, 160, and 200 mA cm^{-2}, respectively) owing to its excellent ion conductivity and selectivity.

As a result of the heavy crossover issue, the PEI and Nafion-PEI membranes could not complete the rate performance test, during which the volumes of the electrolytes on both sides significantly changed.

The Coulombic efficiency (CE), voltage efficiency (VE), and energy efficiency (EE) of the PEI, 25%PBN-PEI, 50%PBN–PEI, 75%PBN-PEI, Nafion 115, and Nafion-PEI are listed in Table S3, Supporting Information. The rate performance of 25%PBN-PEI and 75%PBN-PEI membranes were plotted in Figure S15, Supporting Information. The efficiencies of 50%PBN-PEI and Nafion 115 membrane were further compared (Figure 5b–d). The CE of the membranes increased at a higher rate because of the lower vanadium crossover with shorter charge and discharge times (Figure 5b). The 50%PBN-PEI membranes demonstrated substantially greater CEs (97.16%, 97.44%, 97.72%, 98.14%, 98.55%, 99.07%, and 99.53% at 40, 60, 80, 100, 120,
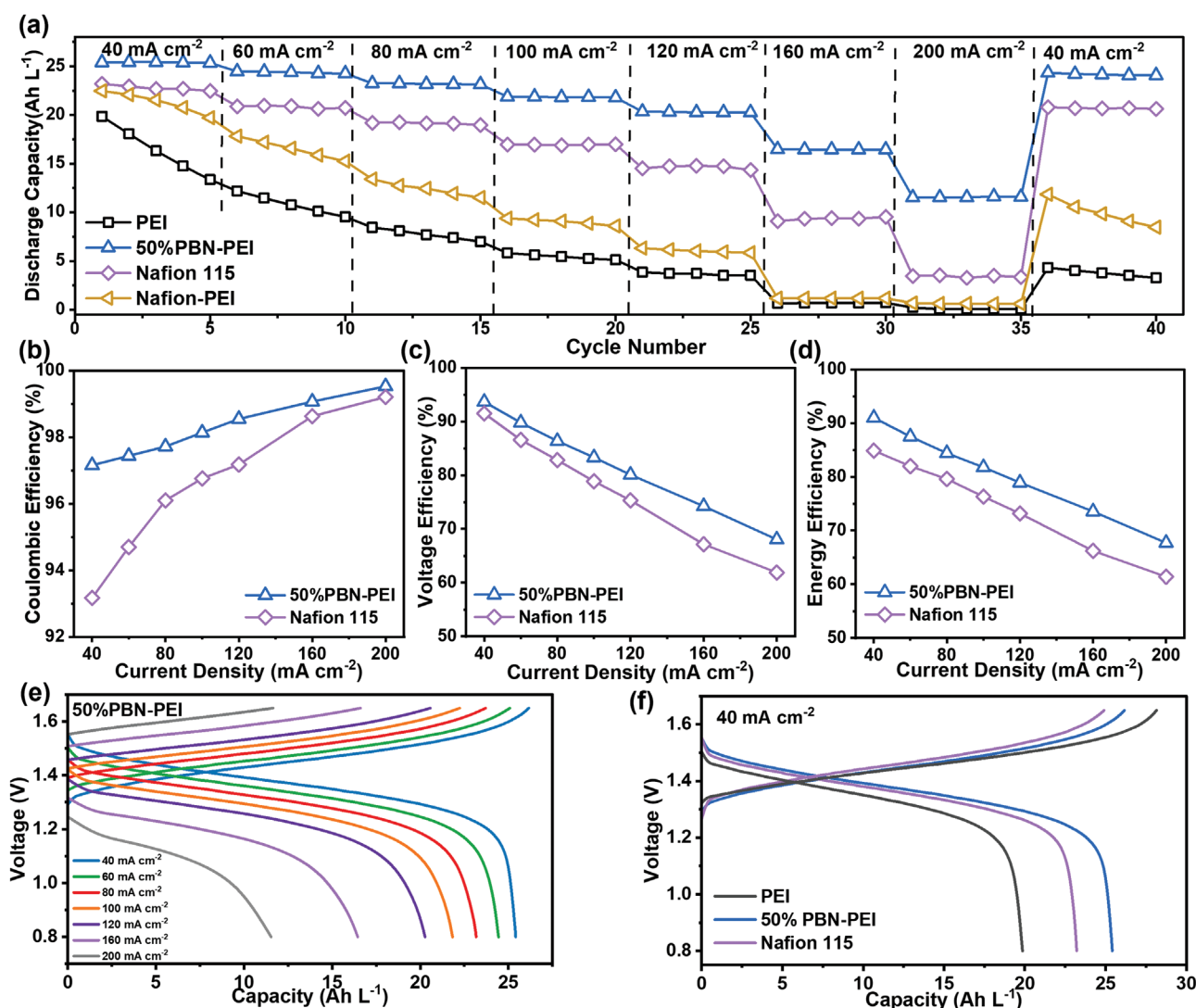

Figure 5. Performance of VRFB assembled by PEI, 50%PBN–PEI, and commercial Nafion 115 membranes. a) Current rate performance of the PEI, 50%PBN–PEI, Nafion 115, and Nafion-PEI membranes at current densities of 40, 60, 80, 100, 120, 160, and 200 mA cm^{-2}. Comparison of b) Coulombic efficiency, c) voltage efficiency, and d) energy efficiency of 50%PBN–PEI and Nafion 115 membranes at different current densities. e) Charge–discharge profiles of 50%PBN–PEI membrane at different current densities. f) Comparison of the charge–discharge profiles of PEI, 50%PBN–PEI, and Nafion 115 membranes at the current density of 40 mA cm^{-2}.

160, and 200 mA cm^{-2}, respectively) than the Nafion 115 membrane, which is consistent with its lower permeability. The VEs of all membranes exhibited a decreasing trend with increasing current density (Figure 5c) because of the increased ohmic loss and electrochemical reaction resistance at higher current densities.[24] For each membrane, the area resistance controlled the ohmic potential drop across the membrane, which further affected the VE.[17] Therefore, the 50%PEI–PBN membrane exhibited superior VE than the Nafion 115 membrane. The EEs are shown in Figure 5d. Consequently, owing to the excellent CE and VE, the 50%PBN–PEI membrane provided the highest EE at all rates (91.00%, 87.50%, 84.41%, 81.77%, 78.94%, 73.55%, and 67.72% at 40, 60, 80, 100, 120, 160, and 200 mA cm^{-2}, respectively). Overall, the 50%PBN–PEI membrane exhibited superior performance compared to the pristine PEI and Nafion 115 membranes.

In order to investigate the electrochemical performance of the 50%PBN–PEI membrane, the charge and discharge profiles at different current densities were plotted (Figure 5e) and compared with the charge and discharge profiles of the pristine PEI and Nafion 115 membranes (Figure 5f). The 50%PBN–PEI membrane exhibited smooth charge and discharge curves at all rates. In comparison with the Nafion 115 membrane, the PEI and 50%PBN–PEI membranes had lower overpotentials during the charging process because of their lower area resistances. During the discharge process, the lowest discharge capacity and voltage of the pristine PEI membrane are ascribed to severe self-discharge.[25] It was observed that the 50%PBN–PEI membrane had higher discharge voltage and larger capacity than the

Nafion 115 membrane, which is more prominent at higher rates (Figure S16, Supporting Information). The impressive performance of the 50%PBN–PEI membrane further confirmed its excellent electrochemical properties.

In order to investigate the stability and long cycling performance of the 50%PBN–PEI membrane, a battery assembled with the membrane was continuously cycled for over 700 cycles at a current density of 100 mA cm^{-2}. As shown in **Figure 6**a, the capacity gradually decayed during cycling owing to the polarization and the migration of the electrolyte from one side to the other side.[26] Therefore, the electrolyte was refreshed every 100 cycles. After that, the capacity of the battery was fully recovered, and the CE, VE, and EE remained stable. This demonstrates that the 50%PBN–PEI membrane has high electrochemical stability. The average capacity fading rate of the 50%PBN–PEI membrane was 0.17% per cycle, which was significantly lower than those of the pristine PEI (1.95% per cycle), Nafion-PEI (1.44% per cycle) and Nafion 115 (0.74% per cycle) membranes because of the higher ion selectivity and lower vanadium permeability. Meanwhile, the hydrophobicity of the PBN layer prevents the migration of the electrolyte. It is observed that CE, VE, and EE are slightly decreased after 700 cycles. This provides a comprehensive result of the aging of several parts of the battery, including the graphite felts, graphite flow fields, and membranes. FTIR spectroscopy was employed to examine the chemical stability of the 50%PBN–PEI membranes. There are no obvious differences between the PBN and PEI layers before and after 100 cycles (Figure 6b,c). The mechanical stability was characterized by a tensile test. The
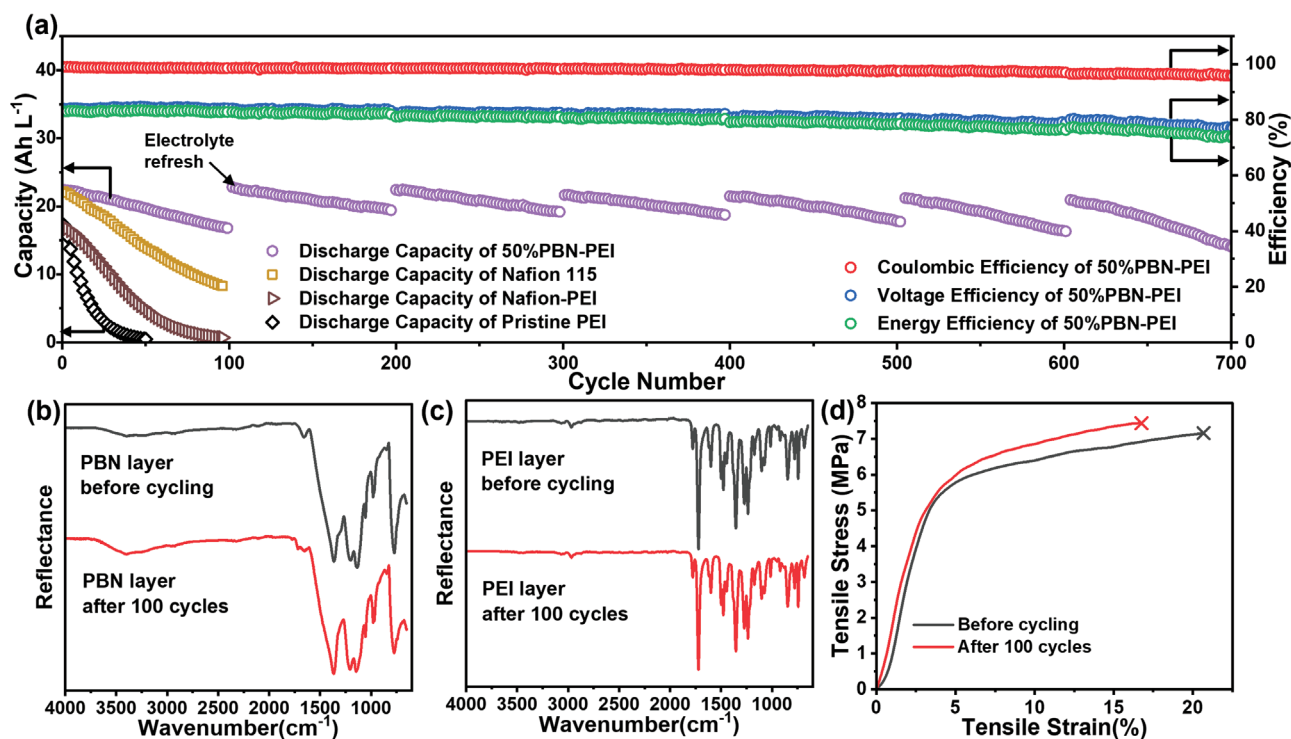
Figure 6. a) Cycling stability in terms of the coulombic, voltage, and energy efficiencies; and discharge capacity of 50%PBN–PEI membrane at the current density of 100 mA cm^{-2}, compared to the discharge–charge capacity of Nafion 115, Nafion-PEI, and pristine PEI membranes. Post-mortem analysis of 50%PBN–PEI membrane before and after cycling in VRFB. FTIR spectra of the b) PBN layer and c) PEI layer before and after cycling. d) Stress–strain curves of the 50%PBN–PEI membrane before and after cycling.

50%PBN–PEI membrane exhibited stable tensile stress after 100 cycles under extreme conditions. Nevertheless, the elongation decreased from 20.68% to 16.33% due to minor deformations during cycling. Overall, the 50%PBN–PEI membrane exhibited excellent stability during long-term cycling.

3. Conclusion

A highly efficient double-layer ion-selective membrane was obtained by integrating the unique properties of porous boron nitride (PBN) with the advantages of the porous polyetherimide (PEI) membranes and Nafion resin. High-nanoporosity PBN flakes were synthesized by a scalable template-free method and further processed for dispersion and functionalization by sonication in isopropanol. During sonication, the B—N bonds near the edges or defects in the amorphous part of PBN were attacked by the solvent molecules and broken into new edges with the hydroxyl and amino groups, which increased the hydrophilicity and crystallinity of PBN. The pore size distribution characterization revealed an ultrahigh micropore and mesopore volume (0.76 cm^3 g^{-1}) of PBN, whereby more than 37% of the pores were smaller than 5 nm, which ensured its high ion selectivity. PBN was further mixed with Nafion resin to form a bifunctional ion-selective layer, which combined the nanoporous structure with the ion-exchange groups. Meanwhile, the inorganic rigid PBN structure suppresses the swelling issue of conventional organic ion-exchange membranes. Through a simple spray-coating process, a PBN ion-selective layer was deposited on a highly ion-conductive and low-cost porous PEI membrane prepared by the NIPS method. The 50%PBN–PEI membrane demonstrated an excellent ion selectivity (1.49×10^8 mS cm^{-3} min) compared with the pristine PEI membrane (6.71×10^6 mS cm^{-3} min) while maintaining its high ion conductivity (64 mS cm^{-1}). The 50%PBN–PEI membrane achieved superior performance than the Nafion 115 membrane in VRFB with higher CE, VE, EE, and capacity at all current densities and high stability with a lower capacity fading rate (0.17% per cycle vs 0.74% per cycle) at 100 mA cm^{-2}. The 50%PBN–PEI membrane also demonstrated a stable operation in VRFB at a current density of 100 mA cm^{-2} over 700 cycles. In summary, the PBN exhibits high ion conductivity and high selectivity owing to its bilayer structure and dual ion conducting approaches. The introduction of the ion-exchange group from Nafion to the unique PBN nanoporous structure further increases the ion conductivity based on dual ion conducting mechanisms. The work presented the remarkable performance of the PBN bifunctional layer in terms of ion conductivity and selectivity; the combination with the low-cost high ion-conductive porous PEI membrane demonstrated a great potential for commercialization of the PBN-PEI double-layer membrane.

4. Experimental Section

Materials: Boric acid (H$_3$BO$_3$, 99.8%, Alfa Aesar) and urea (Certified ACS, Fisher Chemical) were used to synthesize BN. Polyetherimide (PEI, Sigma-Aldrich), polyvinylpyrrolidone (PVP, MW. 40 000, Alfa Aesar), 1-methyl-2-pyrrolidinone (NMP, ≥99%, Sigma-Aldrich) were used for base PEI membrane fabrication. Vanadium (IV) sulfate oxide hydrate (VOSO$_4$, 99.9%, Alfa Aesar) and sulfuric acid (H$_2$SO$_4$, 98.0%, Sigma Aldrich) were used to prepare electrolytes. All chemicals described here were used as received. Nafion perfluorinated resin solution (5 wt%, Sigma-Aldrich) diluted to 1 wt% by isopropanol (IPA, 99.5%, Acros) used for binder in the spray process. The graphite felt (GFD 2, 5 EA, Sigracell) was treated at 400 °C for 30 h in the air and cut into 2.3×2.2 cm^2 used as the electrode. Nafion 115 membrane (Ion Power Inc.) was orderly pretreated in 5 wt% hydrogen peroxide, deionized water, and 1 M sulfuric acid for 1 h of each liquid at 80 °C and then stored in 1 M sulfuric acid before use.

Fabrication of Porous PEI Membrane: 22.5 g PEI and 2.5 g PVP were mixed and dissolved in 75 g NMP solvent at 120 °C for 5 h with magnetic stirring.[10d] The solution was cast on a glass plate at room temperature using the film coater (MSK-AFA-I, MTI) and doctor blade with a thickness of 150 µm. The cast membrane was then immersed in deionized water for 24 h to complete the phase-inversion process and remove the solvent completely.

Synthesis and Treatment of PBN: 0.1 mol boric acid and 0.5 mol urea were solved in 100 mL deionized water and dried in the oven overnight at 105 °C. The dried intermediate was further ground into powders and placed in the tube furnace (OTF-1200X, MTI) heated to 1050 °C (10 °C min^{-1} ramp rate) under nitrogen gas flow (0.05 NI min^{-1}) and held for 3.5 h.[15b] The furnace was then allowed to cool naturally under a nitrogen atmosphere. Pristine PBN was collected after synthesis. 2 g pristine PBN was further ground into powders and then dispersed into 200 mL IPA by sonicating for 4 h. The dispersion was centrifuged for 10 min at 2500 rpm by Sorvall T1 Centrifuge (Thermo Scientific). The PBN in the suspension was further collected by the PTFE filter through vacuum filtration.

Preparation of PBN-PEI Membrane: Different amounts of PBN were dispersed in 4 mL IPA by sonicating for 1 h and then mixed with different amounts of 1 wt% Nafion perfluorinated resin solution by sonicating an additional 10 min to form a uniform suspension. The suspensions were uniformly sprayed on the top surface (waterside in the casting process) of the PEI membrane by airbrush until the surface became wet, and then the membrane was heated on the hotplate (Cimarec+, Thermo Scientific) at 60 °C until the surface became dried. These two processes were repeated until all suspensions were sprayed. All membranes were further treated in deionized water and 1 M sulfuric at 80 °C for 1 h for each liquid and stored in 1 M sulfuric acid before use.

Single Flow Battery Performance: The flow battery was assembled by sandwiching a membrane between four graphite felts, two on each side, clamped by two pieces of graphite flow fields and gold-coating current collectors. In this case, the coated layer of the double-layer membrane was placed on the anode side. The effective area of the electrode and membrane was 5 cm^2. The 1 M VOSO$_4$ and 3 M H$_2$SO$_4$ solution was charged to V$^{3.5+}$ electrolyte for both the cathode and anode sides. The cell was first fully charged the battery at a constant voltage of 1.65 V until the current dropped below 10 mA (Figure S17, Supporting Information) and discharged at a constant current of 200 mA to 0.8 V to complete the initialization. The cycling and rate performance was carried out by the battery test system (CT2001A, LAND, China).

The characterizations and membrane properties measurements methods are shown in the Supporting Information, including SEM, XCT, PSD, XRD, FTIR, TGA, contact angle measurement, water uptake, and swelling measurements, area resistance and ion conductivity measurements, vanadium (IV) permeability and ion selectivity measurements, and tensile strength measurement.

Supporting Information

Supporting Information is available from the Wiley Online Library or from the author.

Conflict of Interest

The authors declare no conflict of interest.

Data Availability Statement

The data that support the findings of this study are available from the corresponding author upon reasonable request.

Keywords

[1] a) Y. Yao, J. Lei, Y. Shi, F. Ai, Y.-C. Lu, *Nat. Energy* **2021**, *6*, 582; b) B. Dunn, H. Kamath, J.-M. J. S. Tarascon, *Science* **2011**, *334*, 928.

[2] P. Leung, X. Li, C. P. De León, L. Berlouis, C. J. Low, F. C. J. R. A. Walsh, *RSC Adv.* **2012**, *2*, 10125.

[3] A. Mukhopadhyay, Y. Yang, Z. Cheng, P. Luan, A. Natan, H. Zhu, *Mater. Today Proc.* **2021**, *13*, 100100.

[4] J. Sheng, A. Mukhopadhyay, W. Wang, H. Zhu, *Mater. Today Proc.* **2019**, *7*, 100044.

[5] a) T. Luo, S. Abdu, M. Wessling, *J. Membr. Sci.* **2018**, *555*, 429; b) L. Liu, C. Wang, Z. He, R. Das, B. Dong, X. Xie, Z. Guo, *J. Mater. Sci. Technol.* **2021**, *69*, 212.

[6] D. W. Shin, M. D. Guiver, Y. M. Lee, *Chem. Rev.* **2017**, *117*, 4759.

[7] Z. Yuan, H. Zhang, X. Li, *Chem. Commun.* **2018**, *54*, 7570.

[8] J. Liu, L. Yu, X. Cai, U. Khan, Z. Cai, J. Xi, B. Liu, F. Kang, *ACS Nano* **2019**, *13*, 2094.

[9] W. Chen, B. Pang, X. Yan, X. Jiang, F. Cui, X. Wu, G. He, *J. Membr. Sci.* **2022**, *644*, 120084.

[10] a) L. Qiao, H. Zhang, W. Lu, Q. Dai, X. Li, *ACS Appl. Mater. Interfaces* **2019**, *11*, 24107; b) D. Chen, D. Li, X. Li, *J. Power Sources* **2017**, *353*, 11; c) Q. Dai, Z. Liu, L. Huang, C. Wang, Y. Zhao, Q. Fu, A. Zheng, H. Zhang, X. Li, *Nat. Commun.* **2020**, *11*, 13; d) Y. Zhao, P. Xiang, Y. Wang, X. Sun, D. Cao, H. Zhu, *J. Membr. Sci.* **2021**, *640*, 119804.

[11] L. Wan, C. Liu, D. Cao, X. Sun, H. Zhu, *ACS Appl. Polym. Mater.* **2020**, *2*, 3001.

[12] a) X.-F. Jiang, Q. Weng, X.-B. Wang, X. Li, J. Zhang, D. Golberg, Y. Bando, *J. Mater. Sci. Technol.* **2015**, *31*, 589; b) W. Lei, D. Portehault, D. Liu, S. Qin, Y. Chen, *Nat. Commun.* **2013**, *4*, 1777; c) P. Singla, N. Goel, S. Singhal, *Ceram. Int.* **2015**, *41*, 10565.

[13] a) X. Wang, C. Zhi, L. Li, H. Zeng, C. Li, M. Mitome, D. Golberg, Y. Bando, *Adv. Mater.* **2011**, *23*, 4072; b) S. Büchele, Z. Chen, E. Fako, F. Krumeich, R. Hauert, O. V. Safonova, N. López, S. Mitchell, J. Pérez-Ramírez, *Angew. Chem.* **2020**, *132*, 19807.

[14] a) S. Schlienger, J. Alauzun, F. Michaux, L. Vidal, J. Parmentier, C. Gervais, F. Babonneau, S. Bernard, P. Miele, J. Parra, *Chem. Mater.* **2012**, *24*, 88; b) P. Dibandjo, L. Bois, F. Chassagneux, D. Cornu, J. M. Letoffe, B. Toury, F. Babonneau, P. Miele, *Adv. Mater.* **2005**, *17*, 571.

[15] a) S. Marchesini, A. Regoutz, D. Payne, C. Petit, *Microporous Mesoporous Mater.* **2017**, *243*, 154; b) S. Marchesini, C. M. McGilvery, J. Bailey, C. Petit, *ACS Nano* **2017**, *11*, 10003; c) A. Nag, K. Raidongia, K. P. Hembram, R. Datta, U. V. Waghmare, C. Rao, *ACS Nano* **2010**, *4*, 1539; d) J. Li, J. Lin, X. Xu, X. Zhang, Y. Xue, J. Mi, Z. Mo, Y. Fan, L. Hu, X. Yang, *Nanotechnology* **2013**, *24*, 155603; e) R. Shankar, S. Marchesini, C. Petit, *J. Phys. Chem. C* **2019**, *123*, 4282; f) A. L'Hermitte, D. M. Dawson, P. Ferrer, K. Roy, G. Held, T. Tian, S. E. Ashbrook, C. Petit, *J. Phys. Chem. C* **2021**, *125*, 27429.

[16] a) A. Hayat, M. Sohail, M. S. Hamdy, T. Taha, H. S. AlSalem, A. M. Alenad, M. A. Amin, R. Shah, A. Palamanit, J. Khan, *Surf. Interfaces* **2022**, 101725; b) J. H. Ramirez Leyva, G. Vitale, A. Hethnawi, A. Hassan, M. J. Perez-Zurita, G. U. Ruiz-Esparza, N. N. Nassar, *ACS Appl. Nano Mater.* **2018**, *1*, 4491.

[17] A. Mukhopadhyay, Z. Cheng, A. Natan, Y. Ma, Y. Yang, D. Cao, W. Wang, H. Zhu, *Nano Lett.* **2019**, *19*, 8979.

[18] a) B. Zou, X. Chang, J. Yang, S. Wang, J. Xu, S. Wang, S. Samukawa, L. Wang, *Prog. Org. Coat.* **2019**, *133*, 139; b) K. Yu, J. Kim, C. Lee, A.-R. Jang, H. S. Shin, K. S. Kim, Y.-J. Yu, E. Choi, *Appl. Phys. Lett.* **2016**, *108*, 241910.

[19] I. M. Joni, R. Balgis, T. Ogi, T. Iwaki, K. Okuyama, *Colloids Surf., A* **2011**, *388*, 49.

[20] a) Y. Lin, T. V. Williams, T.-B. Xu, W. Cao, H. E. Elsayed-Ali, J. W. Connell, *J. Phys. Chem. C* **2011**, *115*, 2679; b) Q. Weng, X. Wang, X. Wang, Y. Bando, D. Golberg, *Chem. Soc. Rev.* **2016**, *45*, 3989.

[21] A. Alghunaim, S. Kirdponpattara, B.-m. Z. Newby, *Powder Technol.* **2016**, *287*, 201.

[22] M. Thommes, K. Kaneko, A. V. Neimark, J. P. Olivier, F. Rodriguez-Reinoso, J. Rouquerol, K. S. Sing, *Pure Appl. Chem.* **2015**, *87*, 1051.

[23] B. Jiang, L. Yu, L. Wu, D. Mu, L. Liu, J. Xi, X. Qiu, *ACS Appl. Mater. Interfaces* **2016**, *8*, 12228.

[24] T. Wang, S. J. Moon, D.-S. Hwang, H. Park, J. Lee, S. Kim, Y. M. Lee, S. Kim, *J. Membr. Sci.* **2019**, *583*, 16.

[25] D. Chen, M. A. Hickner, E. Agar, E. C. Kumbur, *J. Membr. Sci.* **2013**, *437*, 108.

[26] a) Y. Song, X. Li, J. Xiong, L. Yang, G. Pan, C. Yan, A. Tang, *J. Power Sources* **2020**, *449*, 227503; b) Q. Luo, L. Li, W. Wang, Z. Nie, X. Wei, B. Li, B. Chen, Z. Yang, V. Sprenkle, *ChemSusChem* **2013**, *6*, 268.